Energy Conversion and Management 292 (2023) 117419

Contents lists available at ScienceDirect

Energy Conversion and Management

journal homepage: www.elsevier.com/locate/enconman

Resistance-capacitance thermal models as alternatives to finite-element numerical models in the simulation of thermoelectric modules for electric power generation

Alvaro Martinez [a,b]

[a] Department of Engineering, Public University of Navarra, 31006 Pamplona, Spain
[b] Smart Cities Institute, 31006 Pamplona, Spain

ARTICLE INFO

Keywords:
Thermoelectric generator
Thermoelectric module
Resistance–capacitance thermal model
Finite-element software

ABSTRACT

This paper demonstrates that resistance–capacitance models provide equal results than models based on finite-element software when predicting the performance of a thermoelectric module under transient-state conditions. Previous papers on this topic fall short as comparing finite-element models with simplified versions of resistance–capacitance models.

It was confirmed that resistance–capacitance models replicate results of finite-element models in the simulation of a thermoelectric module under steady-state conditions. Deviations lower than 3 % in electric power and efficiency (ratio of electric power to heat input) are obtained for temperature differences between heat source and heat sink as large as 200 K.

Similarly, deviations lower than 3 % are obtained for simulation of a thermoelectric module under transient-state conditions. Resistance-capacitance models not only replicate values, trends and rates of variation predicted by finite-element models under step, linear and sinewave variations in the boundary conditions, but they also do this with negligible computational cost.

1. Introduction

The past decade has witnessed a significant increase in research activities on thermoelectrics. Publications in scientific journals have triple and an increasing number of groups are making contributions around the globe [1]. This is no surprise, given the massive attention gained by thermoelectric applications in a world featuring growing electricity consumption, fossil fuel reservoirs depletion, global warming, and environmental issues [2]. Specially, thermoelectric generators (TEGs) have gained significant momentum given their capacity of producing electric power by harnessing different sources of waste heat [3].

The basic layout of a TEG includes at the core the well-known thermoelectric module (TEM). A TEM is a solid-state device composed of several pairs of different semiconductor materials connected by metal strips, forming an electric circuit. Ceramic layers insulate electrically this circuit and provide mechanical support. When a TEM is sandwiched between a heat source and a heat sink, the temperature difference induces an electromotive force by Seebeck effect that produces electric power in a load resistance connected to it. Therefore, a TEM is just a heat engine that uses electrons as working fluid, so that neither moving parts nor real fluids are needed [4].

Along with one or several TEMs, a TEG includes heat exchangers that connect the TEMs to the heat source and the heat sink. Heat exchangers are also relevant in TEG performance in terms not only of electric power and efficiency, but also in terms of robustness, reliability, and durability [5]. Only when the heat exchangers are also free of moving parts, a TEG achieves maximum levels of these parameters, so as to be part of complex systems working in harsh and remote environments, prohibitive for common mechanical providers of electric power [6].

On the other hand, the main deterrent for TEGs to spread in the market is the low efficiency compared to traditional systems for electric power generation. As an example, a TEG working under a thermal gradient of 120 °C exhibits a conversion efficiency of around 3 %, while systems based on vapour-compression surpass 10 % [7]. That is why TEGs are thought to play a role in applications related to harness free or low-cost heat sources, such as waste heat [8,9], geothermal energy [10,11] or solar radiation [12,13], where the cost of power generation is given mostly by the cost of the equipment.

Great efforts are being made not only on new materials and manufacturing techniques for TEMs [14] and heat exchangers [5], but also on simulation tools for design and optimization [15]. These tools

E-mail address: alvaro.martinez@unavarra.es.

https://doi.org/10.1016/j.enconman.2023.117419
Received 5 April 2023; Received in revised form 13 July 2023; Accepted 14 July 2023
Available online 18 July 2023

Nomenclature

Symbols & acronyms

A	Cross area (m^2)
C	Thermal capacity (J/K)
c	Specific heat ($Jkg^{-1}K^{-1}$)
CFD	Software based on computational fluid dynamics
d	Density (kgm^{-3})
E	Electromotive force (V)
Ef	Efficiency (%)
FEM	Numerical model based on finite-element software
I	Electric current (A)
L	Length (m)
M	Number of nodes representing a leg in a thermoelectric module
N	Number of pairs in a thermoelectric module
P	Electric power (W)
$\dot{Q}$	Heat flow rate (W)
R	Thermal resistance (kW^{-1})
R_L	Electrical load resistance (Ω)
R_0	Electrical resistance of a thermoelectric module (Ω)
RC	Resistance-capacitance thermal model
T	Temperature (K)
t	Time (s)
TEG	Thermoelectric generator
TEM	Thermoelectric module
V	Voltage (V)

Greek letters

α	Seebeck coefficient (VK^{-1})
△ t	Time step (s)
λ	Thermal conductivity ($Wm^{-1}K^{-1}$)
ρ	Electrical resistivity (Ωm)
τ	Thomson coefficient (VK^{-1})

Superscripts

c	External surface of the insulation layer at the cold side
h	External surface of the insulation layer at the hot side
ins	Insulation layer
n	n-type semiconductor leg
p	p-type semiconductor leg
sh	Shunt

are essential to predict the performance of TEGs and properly conduct mechanical, electrical, and thermal optimizations, reducing the need for prototypes, thus saving money and time.

The simulation of TEMs and TEGs is a complex task. TEM simulation, apart from the proper estimation of the Seebeck effect for thermal-electrical conversion, requires the calculation of the temperature distribution in the legs based on Fourier heat, with internal heat generation/absorption determined by Peltier, Joule, and Thomson effects. Therefore, Seebeck coefficient, thermal conductivity, and electrical resistivity of the legs, all of them temperature-dependent, along with the internal structure of legs, contacts, and insulation layers determine the performance of a TEM in terms of power and efficiency [16].

Also, if transient-state simulation is to be conducted, the thermal capacity of all the elements must be added.Finally, the simulation of a complete TEG includes also the heat exchangers since these determine the temperatures at the ends of the TEM. This makes the simulation even more challenging; even a simple finned plate includes spreading/constriction related to the occupancy ratio, conduction in plate and fins, and fin-to-ambient heat convection [17]. Consequently, advanced heat exchangers such as heat pipes, thermosiphons and liquid-cooling systems increase the complexity of the simulation [18], specially under transient-state conditions.

Despite so, the development of computational models for TEM and TEG simulation is considered a case of success, and this development parallels that of prototypes and applications in the last decade [15]. The tools are basically the same than ten years ago, but their predictive power has notably increased.

The seminal classification of simulation models sets them into four categories [19]: the simple model, the improved model, the electric analogy, and the numerical model based on finite-element software (FEM). Lately, researchers have reduced these categories to just two, since the simple and the improved models are simplifications of the electric analogy, as shown in section 2.2. The new category grouping these three models has been renamed as “resistance–capacitance thermal models” (RC), sometimes simplified as “resistance models” [15].

A RC allows the simulation of complete TEGs under transient state [20] with extremely low computational cost. This type of model has been historically called electric analogy given its similarity with electric circuits [19]. In a RC, the TEM is transformed into a heat transfer network of connected nodes or slices, which can be 2-D or 3-D [21], with linear or radial geometry [22,23], although 1-D is usually deployed for TEM simulation [24]. The legs are represented by a variable number of nodes connected by conductive thermal resistances that set the heat transfer among them. These resistances vary independently to each other depending on the local value of the temperature-dependent thermal conductivity. Heat sources/sinks over the corresponding nodes represent internal generation/absorption of heat. The heat produced by Joule effect is calculated at each node depending on the local value of the temperature-dependent electrical resistivity, so it distributes unevenly along the legs. The same applies to the heat by Thomson effect and the temperature-dependent Thomson coefficient. Heat absorption/generation by Peltier effect at either end is determined by a temperature-dependent Seebeck coefficient calculated with the local temperatures at the ends. Apart from legs, shunts and insulation layers can be easily included by extending the network, and even internal or external convection/radiation can be added [21]. The same applies to the heat exchangers [25]. For transient simulation, every node is attached to a capacitor that sets the rate of change of its temperature. The energy balance is applied locally, at every node, which leads to a set of equations easily solved by Gaussian elimination or Gauss-Seidel iteration [20]. The heat transfer network is so similar to an electric circuit that even specific software for electric circuit design, such us SPICE [26,27], has been used to solve the set of equations.

Surprisingly, the literature shows that not advanced but simplified versions of RC are predominant. Among them, there are works on RC reporting only steady-state simulation [24,26–32] by removing the capacitors from the heat transfer network. Others introduce constant thermoelectric properties [21]. However, the simplified RC model most used in the literature is the well-known simple model [4], its extreme simplicity and null computational cost explaining so. The simple model assumes 1-D conductive heat transfer with constant properties calculated at mean temperature of the legs, neglects the Thomson heat, and distributes evenly the heat generated by Joule effect. The simple model represents the legs with just two nodes, one for the hot end and the other for the cold one [33,34], although it can be easily extended to account for contacts and layers [35] and also heat exchangers [36]. It is extensively used in combination with software based on computational fluid dynamics (CFD) for simulation of TEGs with complex heat exchangers [34]. Also, it is present in systems where TEGs are just a subsystem that works in collaboration with many others [37]. As being a RC, the simple model could also be used for transient simulation [3839], although only in the quasistatic form since the capacitors are removed from the heat

transfer network. A quasistatic simulation is a method to approximate transient simulation in situations wherein the boundary conditions change so slow that, at every time instant, the system is considered to be in equilibrium, so steady-state analysis can be applied [40]. On the other hand, the problem is that the simple model has been proven to overestimate electric power and efficiency of a single pair [19] and also of a TEM [41], especially under large temperature differences.

Another simplified RC model is the well-known improved model [42]. It is similar to the simple model except that it considers a temperature-dependent Seebeck coefficient calculated locally at the hot and cold ends of the legs. The Thomson effect is included by a constant Thomson coefficient computed at the mean temperature of the legs. These improvements allow a better estimation of the electromotive force and the Peltier heat. Also, the heat generation/absorption by Thomson effect adds to that by Joule effect, both assumed to distribute evenly along the legs. Again, contacts, layers and heat exchangers are easily included, presenting also an effective coupling with CFD. The improved model adds no complexity to the simple model and provides better results, although still overestimates both electric power and efficiency [19]. Despite so, this model is hardy found in the recent literature in the original form [42], although some works use an equivalent version coming from a modified simple model. It was proven that the simple model with the Seebeck coefficient calculated not at mean temperature but at integrated-mean temperature can be considered an improved model, as it includes a constant Thomson coefficient in the integration [43]. However, this approach is only valid when the temperature along the legs is a linear function of the position, which does not occur for large temperature gradients [16]. Some works can be found computing the whole integral [44,45] or just approximating it [46]. However, in any of its forms, the improved model was also proven to overestimate performance [19,45,47].

Apart from RC, the other big family in thermoelectric simulation is composed of all the models based on FEM. These have been considered the gold standard for TEM and TEG simulation, providing the most reliable and accurate results [15]. Their development has been extraordinary from ten years ago, when the extremely high computational cost limited the use to the simulation of just a single pair under steady state conditions [19]. Nowadays, FEM based on commercial software ANSYS/Fluent and COMSOL allows the simulation of a TEM with complex 3-D structures, including all the thermoelectric effects with temperature-dependent properties and additional effects such as radiation/convection heat transfer in internal and external walls. Also, TEMs and heat exchangers have been coupled in a single FEM to provide simulations for complete TEGs [48].

A big step in this development has taken place quite recently, when a published paper has finally presented a FEM able to simulate a TEM under realistic transient-state conditions. This model, published in [49] and validated in [50], is considered the most reliable and accurate for TEM simulation, according to a recent review [15]. These references indicate that previous attempts have fallen short by either considering just steady-state simulation, or just one thermoelectric pair, or 2-D simulation, or constant thermoelectric properties, or requiring the electric current as input instead of the (more realistic) load resistance. This model has already been extended to include heat exchangers and variable heat sources to compose a transient fluid-thermal-electric multiphysics model [51,52], considered the most complete TEG model ever.

However, the main drawback of this model is the extremely high computational cost. It takes weeks to months to complete a single simulation of a TEG under transient-state conditions, the simulation of the TEMs accounting for around 40 % of this time [52]. Therefore, if several geometries for the TEM are to be tested to find the optimal configuration, multiple simulations must be unavoidably conducted, rendering the task unaffordable in terms of computational cost.

This problem would be partially solved if the TEM were simulated by a RC, as these models present negligible computational cost even for transient simulation [20]. If so, in the simulation of TEGs with heat exchangers so complex that unavoidably require CFD or FEM, at least 40 % of the time would be saved. Also, in those TEGs with simple heat exchangers that require no FEM or CFD at all (wherein analytical or experimental expressions are accurate enough) the whole TEG could be simulated by a RC, allowing for multiple testing with negligible computational cost.

To get so, firstly, RC must show equal accuracy and reliability than FEM in the simulation of a TEM under realistic transient-state conditions. In this regard, comparisons between RC and FEM for TEM simulation are already present in the literature [15]. However, after going through these works, one clearly sees that all of them are conducted between FEM and simplified versions of RC, namely, the simple model [41,52] and the improved model [45]. These works evidently conclude that RC deviate significantly from FEM; but this is a biased statement. The simple and improved models were long ago proven to deviate from FEM even for a single leg [19], and therefore larger deviations are expected when simulating a TEM, an even larger under transient-state simulation.

This conclusion cannot be extended to all RC. In fact, references comparing a FEM and an advanced RC report equal results in the simulation of a thermoelectric pair under steady-state conditions, even for a large temperature difference [19,27]. The point is that there is no paper going further, that is, evaluating whether or not this result also applies when not a pair, but a TEM is simulated, let alone in transient-state conditions, which is a clear gap in the literature that this paper sets out to fill.

Specifically, the main objective of the present paper is to evaluate whether or not an advanced RC is able to replicate the performance of a TEM provided by the most advanced FEM [49], both in steady- and transient-state conditions. This evaluation is of major relevance. The simulation of a TEM with FEM under transient-state conditions takes from days to weeks to be completed so as to provide useful results [52]. When several configurations must be tested to obtain optimal TEM structures, the use of FEM limits the number of alternatives for testing. Conversely, RC provides results within a few seconds. So, if RC were able to replicate results of FEM, a great advance would take place for this technology, as allowing for multiple testing with negligible cost.

To evaluate this, the paper presents in section 2 the materials and methods, namely, the TEM used for comparison, with the properties and geometrical structure of legs, contacts, and insulation layers; the basic theory of RC, with the electrical analogy and the expressions for thermal and electrical parameters applied to this TEM; concluding with the boundary conditions used for comparison. Subsequently, section 3 presents the results and the corresponding discussion; and the paper concludes with section 4, wherein the main outcomes are summarized and commented.

2. Materials and methods

As indicated in section 1, the most advanced model for TEM simulation has been published in [49]. Based on FEM software, it claims to be able to conduct 3-D transient simulation considering temperature-dependent thermoelectric properties and the topological connection of the load resistance, thus outperforming any previous model in the literature. That paper presents steady- and transient-state simulation of a TEM, providing results of power and efficiency under several boundary conditions.

The main objective of the present paper is to compare an advanced RC with the model presented in [49], and evaluate whether or not the advanced RC is able to provide similar results under the same boundary conditions, estimating the deviations between these models. Therefore, the TEM and the boundary conditions used in [49] are taken in the present paper to feed a RC, and the results of power and efficiency obtained in [49] are compared to the results provided by the RC in section 3. The TEM and the boundary conditions are presented in sections 2.1

and 2.3 respectively, whereas section 2.2 describes briefly the structure of the advanced RC.

Since the model in [49] is based on FEM software, this model is named hereafter simply as FEM.

2.1. Thermoelectric module

Reference [49] uses a TEM with 128 pairs of bismuth telluride p-type and n-type semiconductors, connected electrically by copper shunts, and sandwiched between insulation layers based on ceramic materials. Thermal, electrical, and dimensional characteristics of these elements are presented in Table 1.

The authors of [49] also report the temperature-dependent expressions for Seebeck coefficient, thermal conductivity, and electrical resistivity of n-type semiconductors, presented respectively in Eqs. (1)-(3).

$$\alpha^n\ (\mu VK^{-1}) = 1.8027x10^{-7}T^4 - 3.2363x10^{-4}T^3 + 0.2154\ T^2 - 62.9744\ T + 6616.5678 \quad (1)$$

$$\lambda^n\ (Wm^{-1}K^{-1}) = -3.0595x10^{-9}T^4 + 4.5678x10^{-6}T^3 - 2.5162\ x10^{-3}T^2 + 0.6107\ T - 53.9863 \quad (2)$$

$$\rho^n\ (10^{-5}\Omega m) = -3.088x10^{-9}T^4 + 4.5653x10^{-6}T^3 - 2.5854x10^{-3}T^2 + 0.6558\ T - 60.588 \quad (3)$$

If Eq. (1) is plotted versus temperature, one finds the behaviour expected for the Seebeck coefficient of a n-type bismuth telluride, that is, a decrease from ambient temperature to around 350 K and a slight increase for higher temperatures. The same happens with the thermal conductivity of Eq. (2), which shows the expected continuous increase from ambient temperature. However, when plotting Eq. (3) versus temperature, the curve presents a slight increase and then an acute decrease that even provides negative values for temperatures higher than 463 K (190 °C). The broken line in Fig. 1 shows it.

Clearly, Eq. (3) is flawed. The authors provide no reference for it, so no trace can be done. Luckily, a recent paper from these authors [52], wherein the FEM with Eqs. (1)-(3) is deployed and extended, provides a reference for these expressions. It turns out that Eqs. (1)-(3) were obtained experimentally and published in a previous paper [53]. There, the authors calculate experimental values of the thermoelectric properties for different temperatures, plot these values versus temperature, and fit from them Eqs. (1)-(3), which appear explicitly in that paper [53]. On reviewing that, one checks that the plotted curves for Seebeck coefficient and thermal conductivity match perfectly with Eqs. (1) & (2), but this is not the case of the electrical resistivity. Solid line in Fig. 1 shows the electrical resistivity obtained experimentally by the authors (given by Fig. 7 in [53]), which is different to Eq. (3) (broken line). It is clear that the authors made a mistake in the fitting process, which has persisted in subsequent papers [51,52]. Fitted from this solid line, Eq. (4) shows the correct expression for the electrical resistivity.

$$\rho^n\ (10^{-5}\Omega m) = -1.01x10^{-9}T^4 + 1.445x10^{-6}T^3 - 0.8105x10^{-3}T^2 + 0.21519\ T - 19.938 \quad (4)$$

Table 1
Characteristics of the thermoelectric module.

N = 128 pairs	n-type legs (n)	p-type legs (p)	shunts (sh)	insulation layers (ins)
α (μVK^{-1})	Eq. (1)	$\alpha^n = -\alpha^p$	–	–
λ ($Wm^{-1}K^{-1}$)	Eq. (2)	$\lambda^n = \lambda^p$	165.64	22
ρ ($10^{-5}\Omega m$)	Eq. (4)	$\rho^n = \rho^p$	$1.75x10^{-3}$	–
c ($Jkg^{-1}K^{-1}$)	188	$c^n = c^p$	381	850
d (kgm^{-3})	6600	$d^n = d^p$	8978	3600
L (mm)	1	$L^n = L^p$	0.35	0.8
A (mm^2)	1.4x1.4	$A^n = A^p$	3.8x1.4	40x44

2.2. Resistance-capacitance thermal model

Fig. 2 presents the RC that simulates a TEM composed of N thermoelectric pairs of p-type (p) and n-type (n) semiconductor legs, connected thermally in parallel and electrically in series by metallic shunts (sh), and sandwiched between insulation layers (ins). This model derives directly from a previous work [20], wherein one finds a complete description of the model and the equations for the thermoelectric effects. There, each leg was composed of ten nodes, whereas in the present paper, the number of nodes for a single leg (M) is a model input, so equations have been redefined.

All n-type legs are supposed to have equal temperature distribution, so they are grouped into a single branch of M nodes separated an equal distance; the same applies to p-type legs. Shunts at the hot end are included in the first nodes of the legs (n_1, p_1), whereas shunts at the cold end are included in the last nodes (n_M, p_M). Thermal resistances and capacities in n-type legs are calculated with Eqs. (5)-(9). Those for p-type present similar equations (superscript p would substitute superscript n) and are not included for brevity.

$$R^n_{1,2} = \frac{L^n}{(M-1)N\lambda^n_1 A^n} + \frac{L^{sh}}{N\lambda^{sh}A^{sh}/2} \quad (5)$$

$$R^n_{M-1,M} = \frac{L^n}{(M-1)N\lambda^n_{M-1} A^n} + \frac{L^{sh}}{N\lambda^{sh}A^{sh}/2} \quad (6)$$

$$R^n_{i,i+1} = \frac{L^n}{(M-1)N\lambda^n_i A^n}\ i = 2, \cdots, M-2 \quad (7)$$

$$C^n_1 = C^n_M = \frac{NA^nL^nd^nc^n}{M} + NA^{sh}L^{sh}d^{sh}c^{sh}/2 \quad (8)$$

$$C^n_i = \frac{NA^nL^nd^nc^n}{M}\ i = 2, \cdots, M-1 \quad (9)$$

Length, cross area, thermal conductivity, density and specific heat of legs and shunts, as well as number of pairs and number of nodes representing a leg, are model inputs. Thermal conductivity in the legs is included as a temperature-dependent expression and is calculated for each node according to its local temperature. The model allows for different expressions for thermal conductivity in n-type and p-type legs, thus leading to different temperature distribution in n-type and p-type legs. Also, different length and cross area can be used in the legs. None of these features are used in the present paper, since Table 1 indicates that the TEM under simulation presents equal length, cross area and thermal conductivity in n-type and p-type legs.

The network is extended to include the insulation layers. Equal layers are used in both sides, their thermal resistance and capacity given by Eqs. (10) and (11) respectively. Length, cross area, thermal conductivity, density, and specific heat of each layer are model inputs. The external surfaces of these layers are represented by node h at the hot side and node c at the cold side. In this paper, thermal capacities of these nodes (C^h, C^c) are unused as their temperatures (T^h, T^c) are manipulated as boundary conditions (see section 2.3).

$$R^{ins} = \frac{L^{ins}}{\lambda^{ins}A^{ins}} \quad (10)$$

$$C^{ins} = A^{ins}L^{ins}d^{in}c^{ins} \quad (11)$$

Regarding the heat flow rates, Eqs. (12)-(14) present these for the n-type legs. Equations for the p-type legs are similar, so they are not displayed for brevity.

$$\dot{Q}^n_1 = N\left(\frac{-(\alpha^p_1 - \alpha^n_1)T^n_1}{2}I + \rho^n_1 I^2\frac{\frac{L^n}{2M-1}}{A^n} - \tau^n_1 I\frac{T^n_1 - T^n_2}{2}\right) \quad (12)$$

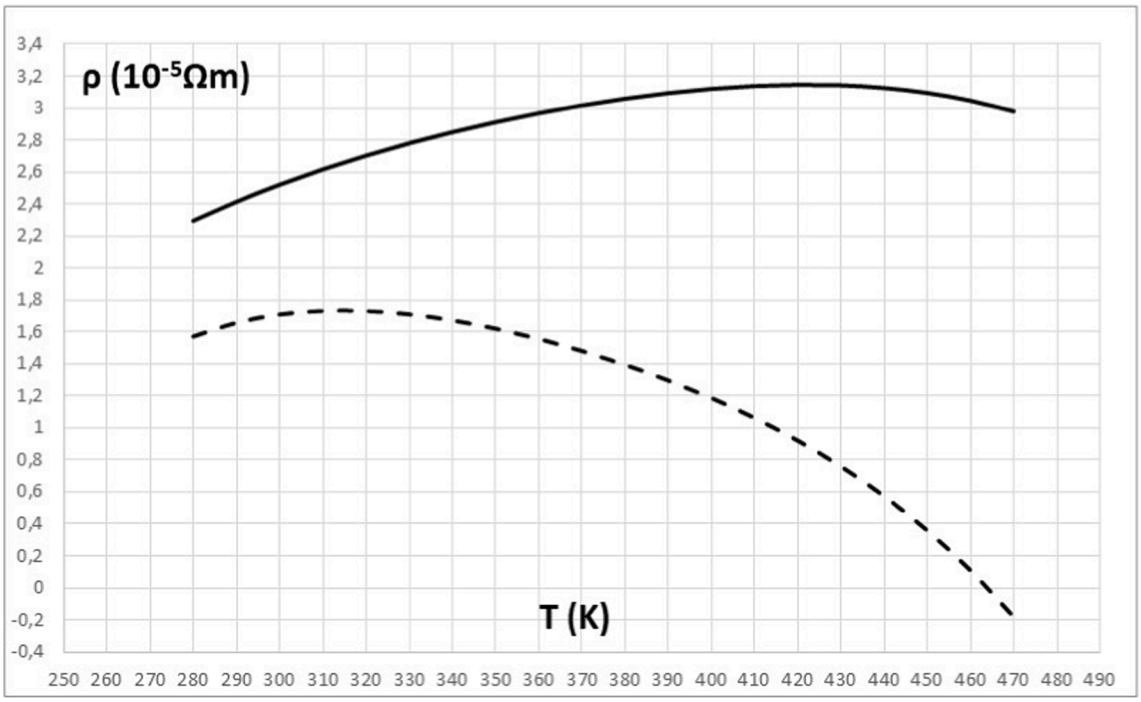

Fig. 1. Electrical resistivity reported in [49] and fitted to Eq. (3) (broken line). Electrical resistivity reported in [53] and fitted to Eq. (4) (solid line).

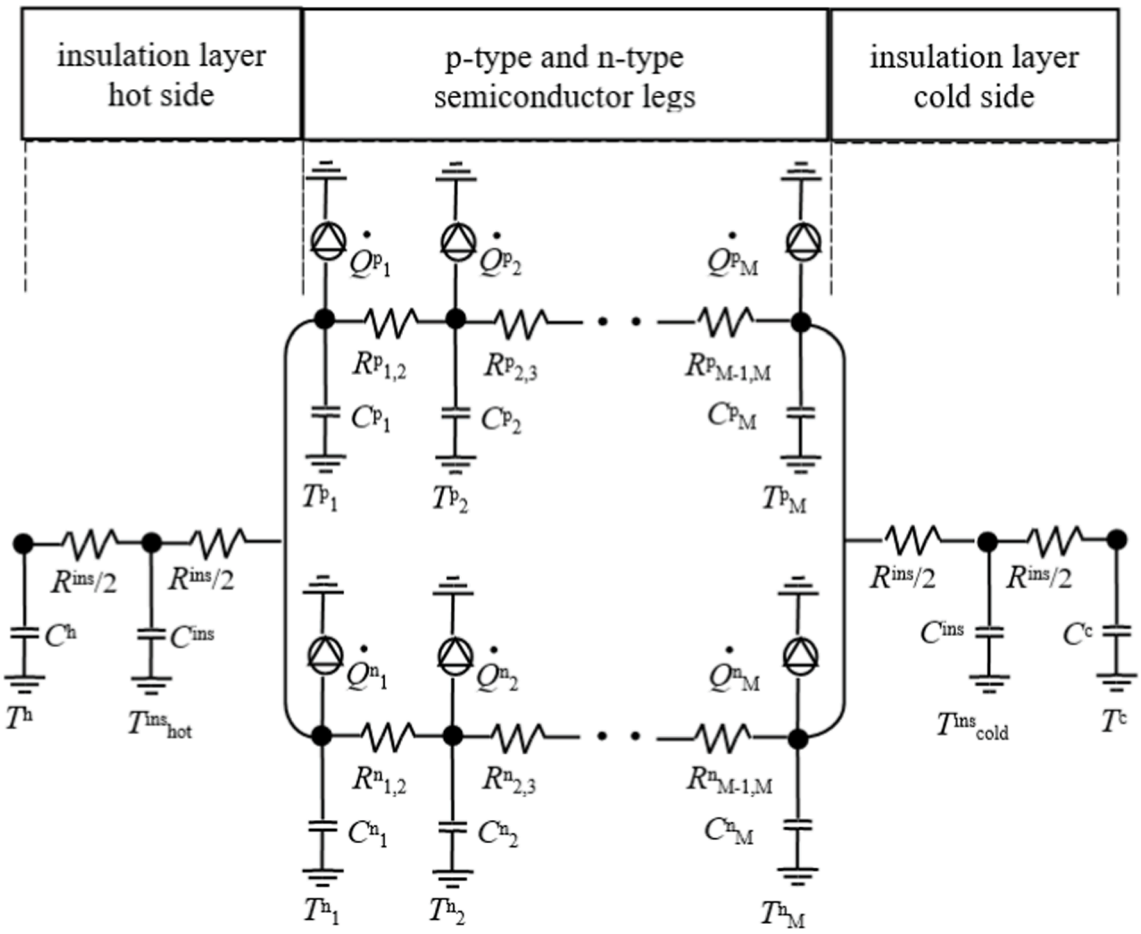

Fig. 2. RC model of a TEM.

$$\dot{Q}_M^n = N\left(\frac{(\alpha_M^p - \alpha_M^n)T_M^n}{2}I + \rho_M^n I^2\frac{\frac{L^n}{M-1}}{A^n} - \tau_M^n I\frac{T_{M-1}^n - T_M^n}{2}\right) \quad (13)$$

$$\dot{Q}_i^n = N\left(\rho_i^n I^2\frac{\frac{L^n}{M-1}}{A^n} - \tau_i^n I\frac{T_{i-1}^n - T_{i+1}^n}{2}\right) i = 2,\cdots,M-1 \quad (14)$$

The first term in Eq. (12) is the heat absorbed by Peltier effect in node n_1, which is calculated using the local temperature (T_1^n) and the local value of the Seebeck effect $(\alpha_1^p - \alpha_1^n)$. This is negative as being an absorbed heat and is just one half because the other half corresponds to node p_1, not presented here. The same applies to the first term in Eq. (13), wherein the positive sign indicates heat generated by Peltier effect at node M.

Heat by Joule effect is generated at every node of the legs and appears in the second term in Eqs. (12) & (13) and in the first term in Eq. (14). This heat is distributed unevenly along the legs, depending on the local value of the electrical resistivity. Heat by Thomson effect applies also to every node of the legs and is represented by the last term in Eqs. (12)-(14). This is also unevenly distributed depending on the temperature distribution along the legs and the local value of the Thomson coefficient, which is derived from the Seebeck coefficient by Eq. (15).

$$\tau = T\frac{d\alpha}{dT} \quad (15)$$

Finally, the electrical resistance of the TEM (R_0) and the electromotive force (E) are given respectively by Eqs. (16) & (17), while Eqs. (18), (19) & (20) provide the voltage (V), electric current (I) and electric power (P) generated by the TEM. Heat absorbed by the TEM at its hot side is calculated with Eq. (21), which allows to determine the efficiency (Ef) with Eq. (22).

$$R_0 = N\left[\frac{\frac{L^n}{M-1}}{A^n}\sum_{i=1}^{M}\rho_i^n + \frac{\frac{L^p}{M-1}}{A^p}\sum_{i=1}^{M}\rho_i^p\right] \quad (16)$$

$$E = N\left[(\alpha_1^p - \alpha_1^n)T_1^n - (\alpha_M^p - \alpha_M^n)T_M^n - \tau_1^p\frac{T_1^p - T_2^p}{2} + \tau_1^n\frac{T_1^n - T_2^n}{2} - \tau_M^p\frac{T_{M-1}^p - T_M^p}{2} + \right.$$
$$\left. + \tau_M^n\frac{T_{M-1}^n - T_M^n}{2} - \sum_{i=2}^{M-1}\left(\tau_i^p\frac{T_{i-1}^p - T_{i+1}^p}{2} - \tau_i^n\frac{T_{i-1}^n - T_{i+1}^n}{2}\right)\right] \quad (17)$$

$$V = E\frac{R_L}{R_L + R_0} \quad (18)$$

$$I = \frac{E}{R_L + R_0} \quad (19)$$

$$P = VI = E^2\frac{R_L}{(R_L + R_0)^2} \quad (20)$$

$$\dot{Q}^h = \frac{T^h - T_{hot}^{ins}}{R^{ins}/2} \quad (21)$$

$$Ef = 100\frac{P}{\dot{Q}^h} \quad (22)$$

Electric parameters, thermal resistances, thermal capacities, and heat flow rates are required to solve the implicit finite-difference expression of the transient-state energy balance [20], which is the basis of RC models. Thus, once all the variables are known at a time instant, along with the temperatures at every node, this expression provides the temperatures after a time step (Δt) and allows to update all the variables for further calculation.

As indicated in section 1, the simple and the improved models are just simplifications of this general RC model. The basic equations of the simple model for simulation of a TEM or just a pair [16,19] are obtained when the thermoelectric properties are considered constants with $\alpha^n = -\alpha^p$, $\lambda^n = \lambda^p$ and $\rho^n = \rho^p$ (therefore, $\tau^n = \tau^p = 0$ and Thomson heat disappears), and the nodes representing the legs are reduced to just two, one for the hot side and the other for the cold side, connected by a single thermal resistance that sets the Fourier heat. As a consequence, each node receives half of the heat by Joule effect. Capacitances are excluded since only the steady state is considered.

Similarly, the basic equations of the improved model appear when applying the same conditions, except for the Seebeck coefficient, which is considered temperature-dependant. This leads to a nonzero Thomson coefficient, introduced as a constant calculated at mean temperature ($\tau^n = -\tau^p$). As a consequence, each node receives half of the heat by Thomson effect added to that by Joule effect.

2.3. Boundary conditions for model comparison and analysis

Several simulations are conducted in [49] to evaluate the performance of the TEM, which are to be replicated with the RC to determine the capacity of the latter to approach the results of the former. In all of them, the boundary conditions are the temperature at the external surface of the insulation layer at the hot side (T^h), that at the cold side (T^c) and the load resistance connected to the TEM (R_L). The outputs that define the performance of the TEM are the electric power (P) and the efficiency (Ef). Values of electric power and efficiency are provided in [49] as graphs and figures. All this information has been extracted by using *WebplotDigitizer* [54].

Table 2 summarizes the studies for comparison and analysis, which are subsequently explained.

In the first place, the authors in [49] conducted a steady-state simulation with T^h set at 450 K, T^c set at 300 K and R_L varying from 0.5 to 10 Ω. This allowed them to determine that the load resistance for maximum power is 4 Ω, known as matched load, this value being fixed for the rest of the simulations. Power and voltage were the outputs provided; efficiency was not provided. This study is to be replicated with RC in the present paper, which has been called study 1.

After that, several simulations were conducted in transient-state conditions. From the results of these, one can also extract steady-state values under different boundary conditions than those in study 1. Therefore, before addressing the transient state, and just to extend the comparison in steady state, power and efficiency are compared for two additional cases, which compose what is called study 2. In both, T^c is set at 300 K, R_L is set at 4 Ω, and T^h is set at 400 K in one test but 500 K in the other.

In all transient-state simulations, T^c was set at 300 K, R_L was set at 4 Ω and T^h varied between 400 and 500 K following different paths. The authors in [49] use always a time step (Δt) of 0.1 s. In the first path, the TEM was stable with T^h = 400 K and this temperature was increased abruptly to 500 K in just one time step. The simulation concluded six seconds later, with all outputs stabilized again. This step increase is to be replicated with RC, which composes study 3. The authors also conducted

Table 2
Boundary conditions in the studies for comparison between RC and [49].

Study	Type	T^h (K)	T^c (K)	R_L (Ω)
1	Steady state	450	300	From 0.5 to 10
2	Steady state	500, 400	300	4
3	Transient state	400 → 500 step	300	4
4	Transient state	400 → 500 linear	300	4
5	Transient state	450 → 500 → 400 → 450 sine wave	300	4

a step decrease from 500 to 400 K, but the results are redundant, and this study is not included in the analysis.

Following this, a linear increase was proposed for T^h. The TEM was stable again with $T^h = 400$ K, this temperature was increased linearly to 500 K in four seconds, and stayed at this value for two additional seconds, when the simulation concluded. This linear increase is to be replicated with RC; this is called study 4. Also, a linear decrease from 500 to 400 K was simulated, but again this study is not included as the results are redundant.

Finally, T^h was simulated as performing a sine wave with a wavelength of eight seconds, starting at 450 K, with 500 and 400 K as maximum and minimum values respectively. This is to be replicated with RC and has been called study 5. The authors also included a triangular wave (linear increase and decrease) equivalent to the sine wave, thus not considered for analysis.

3. Results

Before addressing the five comparative studies of Table 2, the RC is analysed to evaluate how the network influences the results. As indicated in section 2.2, the number of nodes representing a leg (M) is a model input. These nodes are evenly distributed, representing equal lumps of material. The network is composed of 2 M + 4 nodes, as each insulation layer is represented by two nodes (see Fig. 2).

This preliminary test evaluates steady-state results of voltage and power with T^h set at 450 K, T^c set at 300 K and R_L set at 4 Ω. Table 3 provides these results for decreasing M, along with the time consumed for simulation. Variations are calculated by comparison with the case of M = 1000 nodes. All simulations are conducted in MatLab R2020 in a personal computer with Inter® Core™ i5-6300U CPU @ 2.40 GHz and RAM 15.9 GB.

As expected, both accuracy and computational cost decrease for simpler networks. Only 20 nodes per leg are enough to have results deviated less than 1 %. Time reductions are significant, although all of them are negligible compared to computational cost of any model based on FEM. The network selected to conduct the studies of Table 2 is composed of 200 nodes per leg, so the TEM is represented by a network of 404 nodes.

3.1. Comparison under steady-state conditions

Studies 1 & 2 compose the comparison of steady-state performance between RC and FEM. Remember that by FEM, we are referring the model presented in [49], since it is based on FEM software.

3.1.1. Study 1

In the first place, Fig. 3 provides the voltage and the power produced by the TEM under the boundary conditions labelled study 1 in Table 2. The RC (solid lines) replicates with high accuracy the results provided by the FEM (broken lines).

Values of power and efficiency were explicitly provided in [49] for the FEM at $R_L = 4$ Ω. These are presented in columns 2 & 3 of Table 4, first row. Power and efficiency calculated by the RC are also presented in this table for comparison in the row below. Deviations between them are shown in the last row and are calculated with Eq. (23).

$$Deviation(\%) = 100\frac{RC - FEM}{FEM} \tag{23}$$

3.1.2. Study 2

Columns 4 & 5 and 6 & 7 show results for $T^h = 500$ K and 400 K respectively, completing the results of study 1 and confirming the similarity between RC and FEM models in steady-state simulation.

All deviations in power fall below 1.5 %, whereas those for efficiency fall below 3 %. The reason of this extraordinary similarity is very well explained by several figures provided by the authors of [49] on temperature distribution in the TEM during steady-state simulations with FEM. All of them confirm that temperature field highly approximates to 1-D distribution, with equal values in every leg. In other words, 3-D analysis proposed by FEM is not needed for TEM simulation, and consequently RC and FEM are due to provide virtually equal results under the same boundary conditions, confirming what was already obtained long time ago for a single leg [19,27].

3.2. Comparison under transient-state conditions

Studies 3, 4 & 5 compose the comparison of transient-state performance between RC and the model in [49] based on FEM software.

3.2.1. Study 3

Fig. 4 provides power and efficiency for the step increase in T^h. Initially, the TEM is stable with T^h at 400 K when the step takes place at t = 2 s, keeping $T^h = 500$ K until the end of the test.

Regarding the power, one would expect a significant increase in this output once the step occurred, caused by an increase in the temperature difference between the hot and cold shunts, up to the new value of stabilization. This is exactly what both models predict. However, the FEM indicates that the power starts varying even before the step takes place, exactly one second earlier, which is clearly impossible. The authors of [49] acknowledge this flaw, reporting that the FEM software "has undergone smoothing processing through a continuous function". In other words, the model based in FEM software was unable to manage such an acute variation in the boundary conditions and introduced a corrective function that spoiled the simulation at the beginning of the step. This does not occur with the RC, that responds accordingly after the step takes place. Finally, both models show a similar slope for the rate of change during the second part of the step and predict that the new value of stabilization is reached after one second, in t = 3 s.

Regarding the efficiency, this output is defined by Eq. (22) as the ratio of the power and the heat flow rate at the external surface of the insulation layer at the hot side ($\dot{Q}^h$). Applying basic theory of heat transfer [22], this heat can be defined by Eq. (24). In the present work, being constants both the area and the thermal conductivity of the insulation layers, $\dot{Q}^h$ varies only with the temperature gradient around the hot surface of the insulation layer. RC approximates this heat by Eq. (21).

Table 3
Results for the test of network influence on results in RC.

M	Voltage (V)	Power (W)	Time (s)	Variation in voltage (%)	Variation in power (%)	Variation in time (%)
1000	3.7166	3.4533	3.69	–	–	
500	3.7166	3.4533	1.40	0.00	0.00	−62.06
200	3.7166	3.4533	0.55	0.00	0.00	−85.09
100	3.7164	3.4529	0.36	−0.01	−0.01	−90.24
50	3.7154	3.4510	0.33	−0.03	−0.06	−91.06
20	3.7087	3.4386	0.24	−0.21	−0.42	−93.50
10	3.6812	3.3878	0.22	−0.95	−1.90	−94.04
5	3.5374	3.1283	0.20	−4.82	−9.41	−94.58

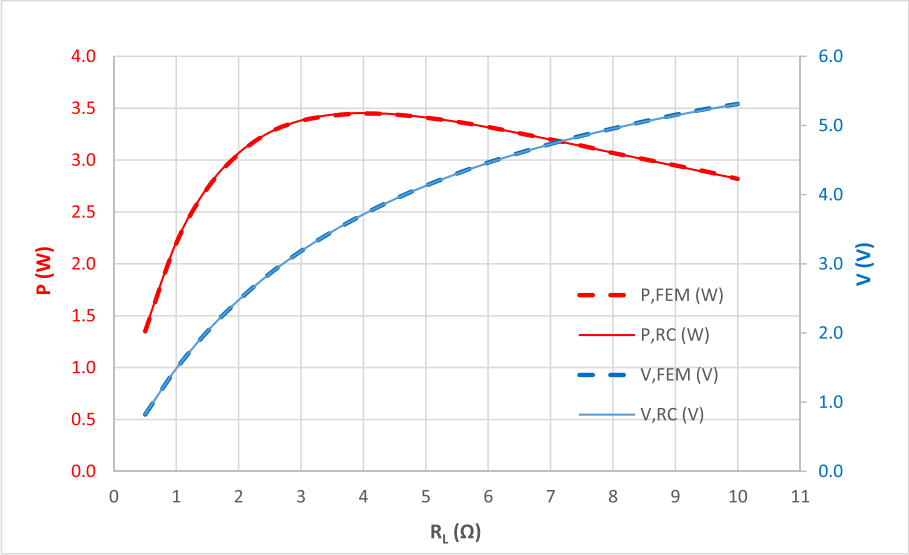

Fig. 3. FEM and RC results of voltage and power for study 1.

Table 4
FEM and RC results of power and efficiency for studies 1 & 2.

	$T^h = 450$ K		$T^h = 500$ K		$T^h = 400$ K	
	P (W)	**Ef (%)**	**P (W)**	**Ef (%)**	**P (W)**	**Ef (%)**
FEM	3.450	2.55	6.040	3.11	1.580	1.92
RC	3.453	2.59	6.120	3.19	1.583	1.93
Deviation (%)	0.09	1.57	1.32	2.64	0.19	0.62

$$\dot{Q}^h = -k^{ins} A^{ins} \left.\frac{\partial T}{\partial L}\right|_h \tag{24}$$

Before discussing the predictions provided by both models, let's analyse which behaviour would be expected. The step would introduce an acute increase in T^h of 100 K in just 0.1 s. It is clear that the only way to produce such an acute increase in T^h is to apply an extremely large $\dot{Q}^h$ during 0.1 s in the hot surface. This intuitive conclusion is confirmed by basic heat transfer analysis as follows. Despite T^h reached 500 K in just 0.1 s, the inner parts of the insulation layer would warm up later, as heat takes some time to flow through them. The consequence would be an immediate and acute increase in the temperature gradient at the hot surface, and therefore an immediate and acute increase in $\dot{Q}^h$. Power would vary later and slower, as heat takes some time to reach the shunts of the hot side. Consequently, one would expect an immediate and acute decrease in the efficiency, followed by a subsequent increase until stabilization.

This pattern is very well predicted by the RC in Fig. 4. The initial value of the efficiency is 1.92 % and it falls down to around 0.6 % when the step takes place to rebound up to the new value of stabilization, that is 3.19 %. The acute increase in $\dot{Q}^h$ introduces a delay of around 0.3 s in the efficiency compared to the power, which makes the former stabilize 0.3 s later than the latter. In this regard, Fig. 5 complement Fig. 4 to explain this behaviour.

In Fig. 5, temperature difference in the hot insulation layer (solid line) approximates the temperature gradient in the hot surface, which correlates with $\dot{Q}^h$. Temperature difference between hot and cold shunts (broken line) correlates with the power. It is clear the acute increase in the former soon after the step takes place, in accordance with previous comments, leading to an immediate and acute increase in $\dot{Q}^h$. On the other hand, the latter varies much more slowly, which explains the slower response of the power. Both explain the spike in the efficiency of

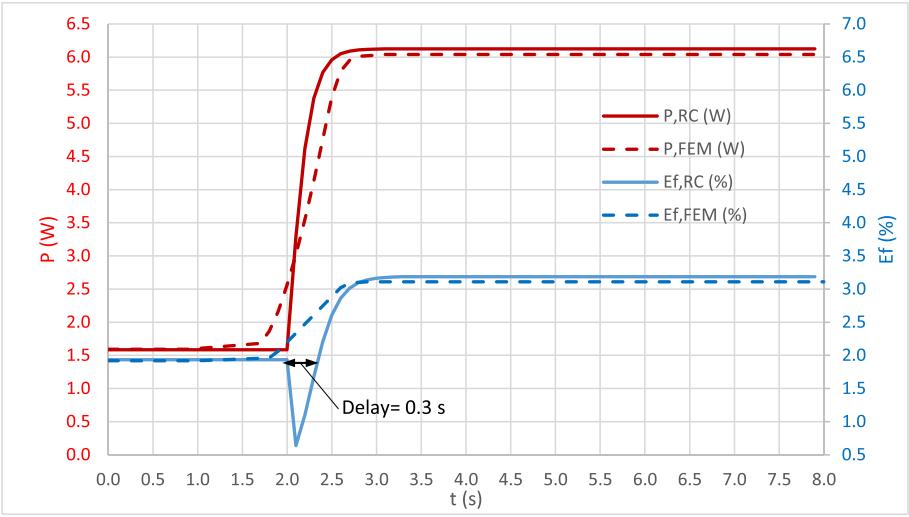

Fig. 4. FEM and RC results of power and efficiency for study 3.

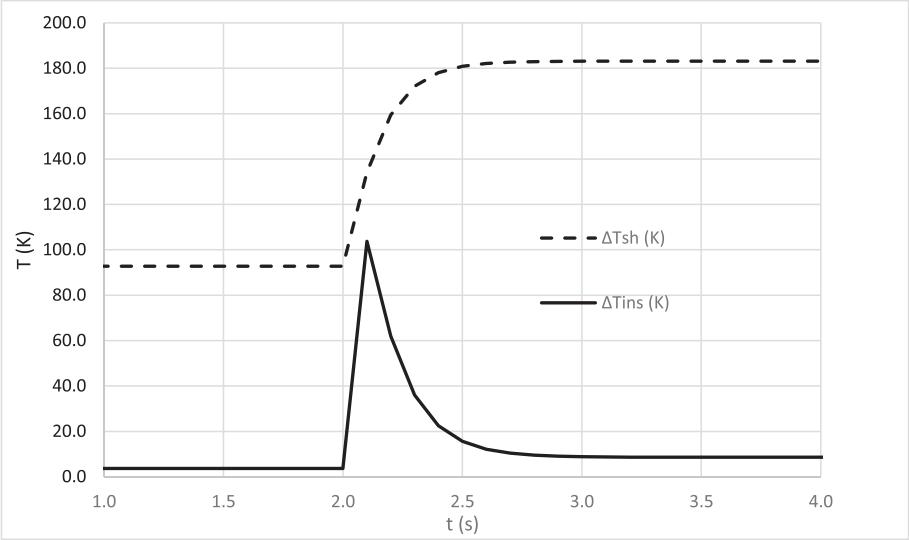

Fig. 5. RC results of temperature difference in the hot insulation layer (solid line) and temperature difference between hot and cold shunts (broken line), for study 3.

Fig. 4 and the corresponding delay.

On the other hand, the simulation of the FEM model in [49] predicts a different behaviour. It not only predicts that the efficiency starts varying before the step takes place, but also that the efficiency copies the pattern of change of the power, thus excluding the cited delay. This seems to be impossible, since, however rapid the response of the power may be, the extremely large $\dot{Q}^h$ needed to increase T^h 100 K in just 0.1 makes the spike unavoidable.

The point is that this behaviour in the efficiency of a TEM under step variations has already been predicted by a model based on FEM sotware in a previous paper [55]. In there, the TEM was composed of a single pair between small ceramic layers, under boundary conditions equal to these in the present paper, namely, matched load, fixed temperature at the cold surface and step variation in the temperature at the hot surface. Power and efficiency exhibited the expected behaviour, with a significant delay between them caused by an initial spike in the efficiency. Moreover, for a pure step increase (wherein T^h presents a vertical increase), the efficiency momentarily fell down to zero as $\dot{Q}^h$ became infinite. In the present paper, having a TEM with N pairs, so N times bigger in size, with thermal capacity N times higher, and under the cited boundary conditions, $\dot{Q}^h$ turns out to be also N times larger, so one would expect a similar pattern of variation.

Looking for a reason for this FEM prediction, apart from the pre-start caused clearly by the smoothing process (in fact, authors in [49] report smoothing correction also for the temperature at the hot shunts), there is one reason that could explain why power and efficiency would present a similar pattern of change. This would happen if the thermal response of the TEM were very fast because of having reduced thermal capacity. If so, the spike would be hidden because of a too-long Δt.

To test so, Fig. 6 presents the efficiency provided by the RC for three cases: solid line shows the efficiency in actual conditions; dotted line shows it for a TEM with thermal capacity (C) ten times lower (Eqs. (8), (9)&(11) divided by ten); and broken line shows it also for a TEM with thermal capacity ten times lower but with $\Delta t = 0.05$ s, half of the value used along this paper.

The dotted line indicates that the TEM must present a thermal capacity at least ten times lower to obtain similar patterns of change in efficiency and power. However, when the time step is reduced, the delay reappears, as the broken line shows. This means that the delay is always there, but a sufficiently short time step is needed to capture it. The TEM

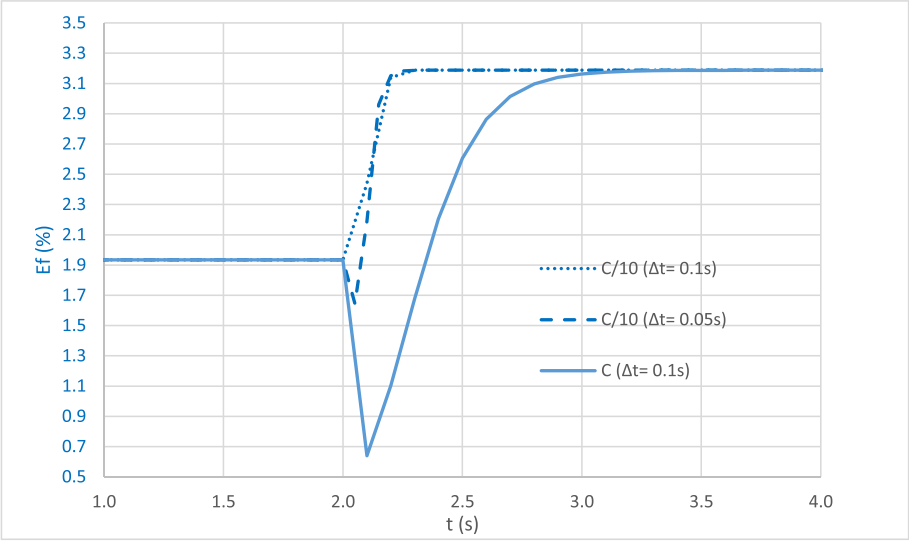

Fig. 6. RC results of efficiency for decreasing TEM thermal capacity and time step, for study 3.

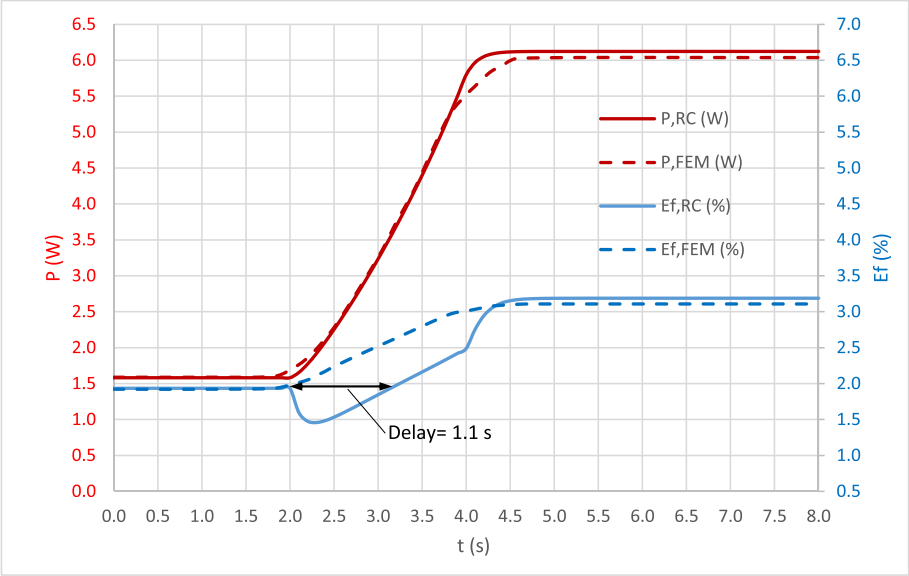

Fig. 7. FEM and RC results of power and efficiency for study 4.

in the present paper presents a thermal capacity of 10.86 J/K, composed of 8.61, 1.63 and 0.62 J/K for layers, shunts, and legs respectively. For these, 0.1 s seems enough to capture the delay, according to RC results.

The conclusion of this study 3 is that RC and FEM provide very similar results in power, apart from the issues of FEM during the initial moments after acute variations in the boundary conditions. On the other hand, no comparison can be done about efficiency, as FEM provides unreasonable results.

3.2.2. *Study 4*

The issues of the FEM model in [49] under the acute change in the boundary conditions in the step increase also appear in the linear-increase simulation, despite the change in boundary conditions is much more relaxed. Fig. 7 provides power and efficiency for the linear increase in T^h. Initially, the TEM is stable with T^h at 400 K when the linear increase starts at t = 2 s and concludes at t = 4 s with T^h = 500 K, maintaining this value until the end of the test.

The smoothing function introduced by the FEM also appears in this case, which makes the power stars varying 0.2 s before the linear increase takes place, whereas the RC responds appropriately. Both present equal rate of change and stabilize at a similar value.

The efficiency requires again a deeper explanation. In this case, the increase in T^h is 100 K in 2 s, which means 5 K every 0.1 s, which is still significant. This linear increase can be considered a step increase of 5 K in 0.1 s, followed by another step increase of 5 K in 0.1 s, and so on. Therefore, according to the comment in section 3.2.1, several spikes in the efficiency would be expected.

To make things a bit clearer, Fig. 8 shows RC results of efficiency and temperature difference in the hot insulation layer for a particular pattern in the variation of T^h. In this particular pattern, T^h is set at 400 K, when a step increase of 5 K is applied in 0.1 s, followed by 0.3 s with T^h set at 405 K, followed by another step increase of 5 K in 0.1 s, followed by 0.3 s with T^h set at 410 K, and so on.

The steps introduce spikes in the temperature difference and, in turn, in $\dot{Q}^h$, leading to corresponding spikes in the efficiency. These spikes are smaller than those in study 3 but still significant to be detected. Then, after eliminating the cited 0.3 s intervals between steps to obtain the original linear increase, one obtains the behaviour of Fig. 7, wherein spikes are blurred by a continuous function.

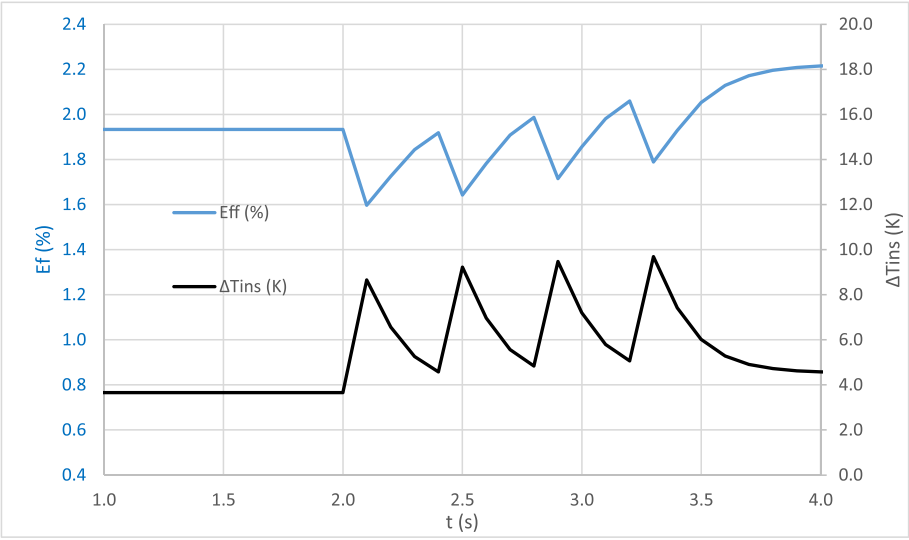

Fig. 8. RC results of efficiency and temperature difference in the hot insulation layer for the particular pattern in the variation of T^h.

RC predicts a delay longer than that in study 3, because T^h varies for a longer interval, but it falls down at a higher value of around 1.5 %. Only after T^h stabilizes, the efficiency catches the power and stabilizes around 3.19 %.

On the other hand, the FEM model in [49] predicts again a similar pattern of change for power and efficiency. This is expected, given that it was unable to capture the spike in efficiency in study 3, wherein the change in the boundary conditions was much more acute than in study 4. It is worth of mention that the cited previous paper [55], which presented a FEM simulation of a small TEM, also provided performance under linear variations in T^h. Power and efficiency predicted by that paper exhibited behaviour in line with these predicted by the RC model in Fig. 7.

Therefore, conclusions of this study liken those in study 3, namely, RC and FEM provide very similar results in power, but no comparison can be done about efficiency, as FEM provides unreasonable results.

3.2.3. Study 5

Finally, Fig. 9 presents power and efficiency for the sinewave variation of T^h. Some open questions raised in previous sections can be explained now.

Regarding the power, both models respond appropriately, presenting equal rate of change and reaching virtually equal maximum and minimum values. More interesting is the fact that the FEM introduces no smoothing function in the simulation. The main difference in the boundary conditions between this case and those in studies 3 & 4 concerns the second derivative of T^h versus t. This derivative is continuous for the sinewave, but it is not for the step and the linear increases. Therefore, one possible explanation for the pre-start with the step and linear increase is that the FEM model has issues when simulating boundary conditions with such characteristic and has to smooth them to make them manageable.

At last, one value can be given to evaluate how close RC and FEM models are in the prediction of the power under transient-state conditions. Fig. 9 shows that the maximum deviation takes place at around t = 2 s, wherein FEM and RC models predict respectively a power of 6.04 and 6.12 W, these values deviated 1.32 % according to Eq. (23).

As for the efficiency, the results of the RC are very well explained by the same arguments than those raised in studies 3 & 4. The rate of change of T^h is smooth because of the sinewave, but it is still significant, the average being 5 K per 0.1 s. This explains why the efficiency, during the initial seconds, follows a pattern similar to that in the linear increase in study 4, which leads to a similar delay respect to power. Contrary to studies 3 & 4, the efficiency never catches the power because the boundary conditions vary during the whole simulation. This explains why the efficiency reaches the maximum and minimum values after the power does so.

Worth of mention is that the maximum and minimum values are different from those in Table 4 for T^h = 500 and 400 K respectively. Again, this is a consequence of the difference in speed of the thermal response of heat and power. As there is a fall in efficiency in the initial moments caused by an acute increase in heat (similar to that seen in studies 3 & 4), there is an acute increase in efficiency after T^h starts falling in t = 2 s, caused by an acute decrease in heat. Power responds later, so the efficiency still goes up until t = 4 s. The same applies when T^h starts increasing again in t = 6 s.

On the other hand, unreasonable results are again provided by the FEM model in [49]. There is no smoothing function in this case. There is just one clue that can explain this behaviour and arises from a quote by the authors in [49], who explicitly indicate that "Here, the heat absorption is equal to Fourier heat plus hot side Peltier heat and minus one half of the Joule heat…" In other words, to calculate $\dot{Q}^h$ (called "absorbed heat"), they are using the steady-state energy balance applied at the hot side of a TEM.

The point is this expression can be used only to conduct calculations under steady-state conditions [4,16], but it is useless for transient state. This expression considers that the TEM is always in equilibrium, thus neglecting the influence of time [22]. Therefore, the authors are introducing a steady-state condition to calculate $\dot{Q}^h$ and, in turn, the efficiency. As a consequence, these are not calculated under transient-state conditions, but under what is called quasistatic conditions.

As indicated in section 1, a quasistatic simulation is a method to approximate transient simulation in situations wherein the boundary conditions change so slow that, at every time instant, the system is considered to be in equilibrium, so steady-state analysis can be applied [40]. This explains not only why power and efficiency follow similar patterns in the present paper, but also why both reach exactly the steady-state values of Table 4. The problem is that quasistatic simulation cannot be applied to the present TEM under such acute variations in the boundary conditions, rendering efficiency results useless for study and comparison with those of the RC model.

Again, the FEM presented in the cited previous paper [55] was able to perform real transient-state simulation, calculating $\dot{Q}^h$ perfectly according to Eq. (24) at every time instant with coherent results. Therefore, it seems that there are issues extending a model based on FEM

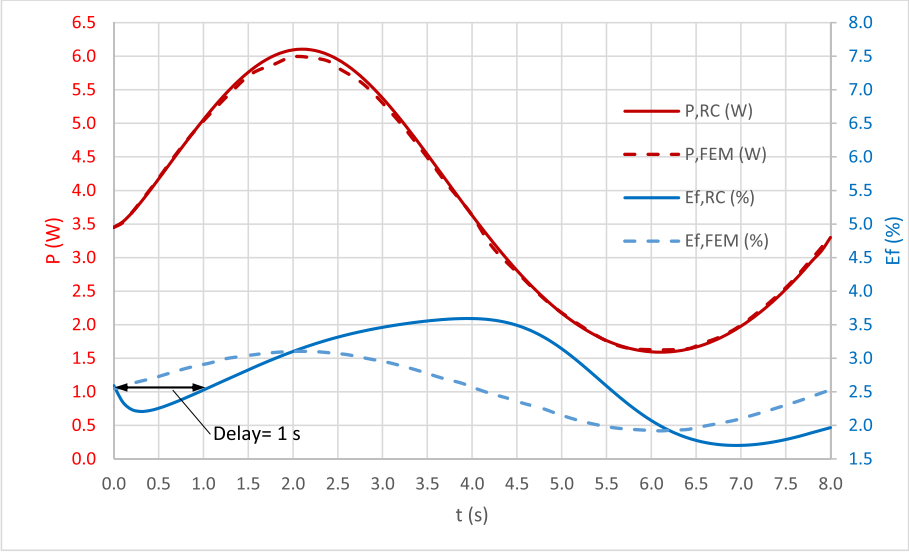

Fig. 9. FEM and RC results of power and efficiency for study 5.

software for the simulation of a TEM with several pairs.

4. Conclusions

This paper was initially conceived to evaluate whether or not a resistance–capacitance model (RC) is able to replicate results of a finite-element-based numerical model (FEM) in the simulation of a thermoelectric module (TEM) under steady- and transient-state conditions. The literature presents transient-state comparisons of FEM with simplified RC versions, and no one presents it for an advanced RC.

For the comparison, it has been selected a model based on FEM software recently published, which is considered the most advanced, reliable, and accurate up to now. However, this model presents some issues in the simulation of power and efficiency that have limited the scope of the comparison under transient-state conditions.

In the first place, FEM and RC are compared in steady-state conditions, providing electric power and efficiency under different boundary conditions. RC is able to replicate FEM results of power with deviations lower than 1.5 % in all the cases, and those for efficiency are lower than 3 %. Also, they provide equal curves of power and efficiency versus load resistance under equal boundary conditions.

As for the transient state, the model based on FEM presents two serious difficulties that avoid a proper comparison with RC.

The first issue is that it is unable to deal with acute variations in the boundary conditions, so that smoothing functions must be included. These lead to impossible results, such as an electric power that varies even before the change in boundary conditions has occurred. This issue is not present in the simulation with RC. When boundary conditions are not so acute and the model based on FEM is able to manage them, RC replicates values, trends and rates of variation predicted by it. Maximum deviation of 1.5 % is found when providing values of electric power under sinewave variation in the boundary conditions.

The second issue is that the model based on FEM is not able to provide the efficiency by real transient-state simulation, but it introduces an approximation by conducting quasistatic simulation. This type of simulation is useless for rapid variations in the boundary conditions, such as those in this paper, so unrealistic results of efficiency are provided. This precludes any comparison with RC. On the other hand, RC does not present such issue and provides results of efficiency in line with the literature of transient-state simulation for simple TEMs.

In summary, according to these results, recommendations for thermoelectric simulation should be reformulated. Models based on FEM are unarguably the best option for the simulation of a thermoelectric pair in steady- and transient-state conditions. On the other hand, RC is preferred for a complete generator, and this claim is much more applicable when transient simulation is to be conducted. Finally, for the simulation of a TEM, models based on FEM have historically been considered the gold standard, though this claim is valid only for steady-state simulation, according to the present paper.

In brief, with the information available up to now, RC can be considered an accurate and reliable alternative to model based on FEM in the simulation of a TEM. Moreover, they are cost-effective in terms of computational time, as transient-state simulation is conducted within seconds, whereas FEM takes days to weeks.

It is clear that the cited issues have limited the scope of comparison. Refined models based on FEM are expected to deal with such issues and provide new information for analysis and comparison.

Declaration of Competing Interest

The authors declare that they have no known competing financial interests or personal relationships that could have appeared to influence the work reported in this paper.

Data availability

Data will be made available on request.

Acknowledgements

The authors acknowledge the support of the Spanish Ministry of Science, Innovation and Universities, and the European Regional Development Fund, under grant PID2021-124014OB-I00 (VIVOTEG). Open access funding provided by Universidad Pública de Navarra.

References

[1] Wu Z, Zhang S, Liu Z, Mu E, Hu Z. Thermoelectric converter: Strategies from materials to device application. Nano Energy 2022;91:106692. https://doi.org/10.1016/j.nanoen.2021.106692.
[2] Tohidi F, Ghazanfari Holagh S, Chitsaz A. Thermoelectric Generators: A comprehensive review of characteristics and applications. Appl Therm Eng 2022;201:117793. https://doi.org/10.1016/j.applthermaleng.2021.117793.
[3] Alghoul M, Shahahmadi S, Yeganeh B, Asim N, Elbreki A, Sopian K, et al. A review of thermoelectric power generation systems: roles of existing test rigs/ prototypes and their associated cooling units on output performance. Energy Convers Manage 2018;174:138–56. https://doi.org/10.1016/j.enconman.2018.08.019.
[4] Ioffe A. Semiconductor thermoelements and thermo-electric cooling. London: Infosearch Ltd.; 1954.
[5] Patil D, Arakerimath R, Walke P. Thermoelectric materials and heat exchangers for power generation – a review. Renew Sustain Energy Rev 2018;95:1–22. https://doi.org/10.1016/j.rser.2018.07.003.
[6] Hammel T, Bennett R, Sievers B. Evolutionary upgrade for the multi-mission radioisotope thermoelectric generator (MMRTG). 2016 IEEE Aerospace Conference, vol. 2016- June, IEEE; 2016, p. 1–8. https://doi.org/10.1109/AERO.2016.7500748.
[7] Astrain D, Jaramillo-Fernandez J, Araiz M, Francone A, Catalán L, Jacobo-Martín A, et al. Enhanced behaviour of a passive thermoelectric generator with phase change heat exchangers and radiative cooling. Appl Therm Eng 2023;225:120162. https://doi.org/10.1016/j.applthermaleng.2023.120162.
[8] Burnete N, Mariasiu F, Depcik C, Barabas I, Moldovanu D. Review of thermoelectric generation for internal combustion engine waste heat recovery. Prog Energy Combust Sci 2022;91:101009. https://doi.org/10.1016/j.pecs.2022.101009.
[9] Sun T, Wang L, Jiang W. Pushing thermoelectric generators toward energy harvesting from the human body: challenges and strategies. Mater Today 2022;57:121–45. https://doi.org/10.1016/j.mattod.2022.06.001.
[10] Catalán L, Araiz M, Aranguren P, Padilla G, Hernandez P, Perez N, et al. Prospects of autonomous volcanic monitoring stations: experimental investigation on thermoelectric generation from fumaroles. Sensors 2020;20:3547. https://doi.org/10.3390/s20123547.
[11] Alegría P, Catalán L, Araiz M, Rodríguez A, Astrain D. Experimental development of a novel thermoelectric generator without moving parts to harness shallow hot dry rock fields. Appl Therm Eng 2022;200:117619. https://doi.org/10.1016/j.applthermaleng.2021.117619.
[12] Narducci D, Lorenzi B. Hybrid thermoelectric-photovoltaic solar harvesters: technological and economic issues. Jpn J Appl Phys 2022;62:SD0801. https://doi.org/10.35848/1347-4065/aca031.
[13] Karthick K, Suresh S, Hussain M, Ali H, Kumar C. Evaluation of solar thermal system configurations for thermoelectric generator applications: a critical review. Sol Energy 2019;188:111–42. https://doi.org/10.1016/j.solener.2019.05.075.
[14] Beretta D, Neophytou N, Hodges J, Kanatzidis M, Narducci D, Martin- Gonzalez M, et al. Thermoelectrics: from history, a window to the future. Mater Sci Eng R Rep 2019;138:100501. https://doi.org/10.1016/j.mser.2018.09.001.
[15] Luo D, Liu Z, Yan Y, Li Y, Wang R, Zhang L, et al. Recent advances in modeling and simulation of thermoelectric power generation. Energy Convers Manag 2022;273:116389. https://doi.org/10.1016/j.enconman.2022.116389.
[16] Angrist S. Thermoelectric Generators. Direct Energy Conversion. 2th ed., Boston: Allyn and Bacon, Inc.; 1971, p. 122–86.
[17] Aranguren P, Astrain D, Rodríguez A, Martínez A. Net thermoelectric power generation improvement through heat transfer optimization. Appl Therm Eng 2017;120:496–505. https://doi.org/10.1016/j.applthermaleng.2017.04.022.
[18] Araiz M, Martínez A, Astrain D, Aranguren P. Experimental and computational study on thermoelectric generators using thermosyphons with phase change as heat exchangers. Energy Convers Manage 2017;137:155–64. https://doi.org/10.1016/j.enconman.2017.01.046.
[19] Fraisse G, Ramousse J, Sgorlon D, Goupil C. Comparison of different modeling approaches for thermoelectric elements. Energy Convers Manage 2013;65:351–6. https://doi.org/10.1016/j.enconman.2012.08.022.
[20] Martínez A, Astrain D, Rodríguez A. Dynamic model for simulation of thermoelectric self cooling applications. Energy 2013;55:1114–26. https://doi.org/10.1016/j.energy.2013.03.093.
[21] Nozariasbmarz A, Suarez F, Dycus J, Cabral M, LeBeau J, Ozturk M, et al. Thermoelectric generators for wearable body heat harvesting: Material and device concurrent optimization. Nano Energy 2020;67:104265. https://doi.org/10.1016/j.nanoen.2019.104265.
[22] Chapman A. Heat Transfer. 4th ed. Prentice Hall; 1984.

[23] Shen Z, Liu X, Chen S, Wu S, Xiao L, Chen Z. Theoretical analysis on a segmented annular thermoelectric generator. Energy 2018;157:297–313. https://doi.org/10.1016/j.energy.2018.05.163.
[24] Rodríguez A, Vián J, Astrain D, Martínez A. Study of thermoelectric systems applied to electric power generation. Energy Convers Manag 2009;50:1236–43. https://doi.org/10.1016/j.enconman.2009.01.036.
[25] Martínez A, Vián J, Astrain D, Rodríguez A, Berrio I. Optimization of the heat exchangers of a thermoelectric generation system. J Electron Mater 2010;39:1463–8. https://doi.org/10.1007/s11664-010-1291-4.
[26] Mitrani D, Salazar J, Turó A, García M, Chávez J. One-dimensional modeling of TE devices considering temperature-dependent parameters using SPICE. Microelectronics J 2009;40:1398–405. https://doi.org/10.1016/j.mejo.2008.04.001.
[27] Chen M, Rosendahl L, Condra T, Pedersen J. Numerical modeling of thermoelectric generators with varing material properties in a circuit simulator. IEEE Trans Energy Convers 2009;24:112–24. https://doi.org/10.1109/TEC.2008.2005310.
[28] Alegría P, Catalán L, Araiz M, Casi A, Astrain D. Thermoelectric generator for high temperature geothermal anomalies: experimental development and field operation. Geothermics 2023:110. https://doi.org/10.1016/j.geothermics.2023.102677.
[29] Casi A, Araiz M, Catalán L, Astrain D. Thermoelectric heat recovery in a real industry: from laboratory optimization to reality. Appl Therm Eng 2021;184:116275. https://doi.org/10.1016/j.applthermaleng.2020.116275.
[30] Araiz M, Casi A, Catalán L, Martínez A, Astrain D. Prospects of waste-heat recovery from a real industry using thermoelectric generators: Economic and power output analysis. Energy Convers Manag 2020;205:112376. https://doi.org/10.1016/j.enconman.2019.112376.
[31] Aranguren P, Astrain D, Rodríguez A, Martínez A. Experimental investigation of the applicability of a thermoelectric generator to recover waste heat from a combustion chamber. Appl Energy 2015;152:121–30. https://doi.org/10.1016/j.apenergy.2015.04.077.
[32] Shen Z, Wu S, Xiao L, Yin G. Theoretical modeling of thermoelectric generator with particular emphasis on the effect of side surface heat transfer. Energy 2016;95:367–79. https://doi.org/10.1016/j.energy.2015.12.005.
[33] Stevens J. Optimal design of small Delta-T thermoelectric generation systems. Energy Convers Manag 2001;42:709–20. https://doi.org/10.1016/S0196-8904(00)00099-6.
[34] Massaguer E, Massaguer A, Montoro L, Gonzalez J. Development and validation of a new TRNSYS type for the simulation of thermoelectric generators. Appl Energy 2014;134:65–74. https://doi.org/10.1016/j.apenergy.2014.08.010.
[35] Rowe D, Min G. Design theory of thermoelectric modules for electrical power generation. IEE Proc. – Sci., Measur. Technol. 1996;143:351. https://doi.org/10.1049/ip-smt:19960714.
[36] Henderson J. Analysis of a heat exchanger-thermoelectric generator system. 14th Intersociety Energy Conversion Eng Conf 1979;2:1835–40.
[37] Demir M, Dincer I. Development of an integrated hybrid solar thermal power system with thermoelectric generator for desalination and power production. Desalination 2017;404:59–71. https://doi.org/10.1016/j.desal.2016.10.016.
[38] Lan S, Yang Z, Chen R, Stobart R. A dynamic model for thermoelectric generator applied to vehicle waste heat recovery. Appl Energy 2018;210:327–38. https://doi.org/10.1016/j.apenergy.2017.11.004.
[39] Gou X, Yang S, Xiao H, Ou Q. A dynamic model for thermoelectric generator applied in waste heat recovery. Energy 2013;52:201–9. https://doi.org/10.1016/j.energy.2013.01.040.
[40] Díaz de Garayo S, Martínez A, Astrain D. Annual energy performance of a thermoelectric heat pump combined with a heat recovery unit to HVAC one passive house dwelling. Appl Therm Eng 2022;204:117832. https://doi.org/10.1016/j.applthermaleng.2021.117832.
[41] Meng J, Zhang X, Wang X. Characteristics analysis and parametric study of a thermoelectric generator by considering variable material properties and heat losses. Int J Heat Mass Transf 2015;80:227–35. https://doi.org/10.1016/j.ijheatmasstransfer.2014.09.023.
[42] Chen J, Yan Z, Wu L. The influence of Thomson effect on the maximum power output and maximum efficiency of a thermoelectric generator. J Appl Phys 1996;79:8823. https://doi.org/10.1063/1.362507.
[43] Sandoz-Rosado E, Weinstein S, Stevens R. On the Thomson effect in thermoelectric power devices. Int J Therm Sci 2013;66:1–7. https://doi.org/10.1016/j.ijthermalsci.2012.10.018.
[44] Armstrong H, Boese M, Carmichael C, Dimich H, Seay D, Sheppard N, et al. Estimating energy conversion efficiency of thermoelectric materials: constant property versus average property models. J Electron Mater 2017;46:6–13. https://doi.org/10.1007/s11664-016-4890-x.
[45] Luo D, Wang R, Yu W. Comparison and parametric study of two theoretical modeling approaches based on an air-to-water thermoelectric generator system. J Power Sources 2019;439:227069. https://doi.org/10.1016/j.jpowsour.2019.227069.
[46] Fan L, Zhang G, Wang R, Jiao K. A comprehensive and time-efficient model for determination of thermoelectric generator length and cross-section area. Energy Convers Manage 2016;122:85–94. https://doi.org/10.1016/j.enconman.2016.05.064.
[47] Ponnusamy P, de Boor J, Müller E. Using the constant properties model for accurate performance estimation of thermoelectric generator elements. Appl Energy 2020;262:114587. https://doi.org/10.1016/j.apenergy.2020.114587.
[48] Massaguer A, Massaguer E, Comamala M, Pujol T, González J, Cardenas M, et al. A method to assess the fuel economy of automotive thermoelectric generators. Appl Energy 2018;222:42–58. https://doi.org/10.1016/j.apenergy.2018.03.169.
[49] Luo D, Yan Y, Wang R, Zhou W. Numerical investigation on the dynamic response characteristics of a thermoelectric generator module under transient temperature excitations. Renew Energy 2021;170:811–23. https://doi.org/10.1016/j.renene.2021.02.026.
[50] Luo D, Wang R, Yu W, Zhou W. Parametric study of a thermoelectric module used for both power generation and cooling. Renew Energy 2020;154:542–52. https://doi.org/10.1016/j.renene.2020.03.045.
[51] Luo D, Wang R, Yan Y, Yu W, Zhou W. Transient numerical modelling of a thermoelectric generator system used for automotive exhaust waste heat recovery. Appl Energy 2021;297:117151. https://doi.org/10.1016/j.apenergy.2021.117151.
[52] Luo D, Zhao Y, Yan Y, Chen H, Chen W, Wang R, et al. Development of two transient models for predicting dynamic response characteristics of an automobile thermoelectric generator system. Appl Therm Eng 2023;221:119793. https://doi.org/10.1016/j.applthermaleng.2022.119793.
[53] Luo D, Wang R. Experimental test and estimation of the equivalent thermoelectric properties for a thermoelectric module. J Energy Resour Technol 2021;143. https://doi.org/10.1115/1.4050132.
[54] Rohatgi A. WebPlotDigitizer 2022.
[55] Meng J, Zhang X, Wang X. Dynamic response characteristics of thermoelectric generator predicted by a three-dimensional heat-electricity coupled model. J Power Sources 2014;245:262–9. https://doi.org/10.1016/j.jpowsour.2013.06.127.